Imaging-Guided Gene Therapy of Experimental Gliomas

Andreas H. Jacobs, Maria Adele Rueger, Alexandra Winkeler, Hongfeng Li, Stefan Vollmar, Yannic Waerzeggers, Benedikt Rueckriem, Christiane Kummer, Claus Dittmar, Markus Klein, Michael T. Heneka, Ulrich Herrlinger, Cornel Fraefel, Rudolf Graf, Klaus Wienhard, and Wolf-Dieter Heiss

Laboratory for Gene Therapy and Molecular Imaging at the Max Planck Institute for Neurological Research, Center for Molecular Medicine, and Department of Neurology, University of Cologne, Cologne, Germany

Abstract

To further develop gene therapy for patients with glioblastomas, an experimental gene therapy protocol was established comprising a series of imaging parameters for (*i*) noninvasive assessment of viable target tissue followed by (*ii*) targeted application of herpes simplex virus type 1 (HSV-1) amplicon vectors and (*iii*) quantification of treatment effects by imaging. We show that viable target tissue amenable for application of gene therapy vectors can be identified by multitracer positron emission tomography (PET) using 2-^{18}F-fluoro-2-deoxy-D-glucose, *methyl*-^{11}C-L-methionine, or 3′-deoxy-3′-^{18}F-fluoro-L-thymidine ([^{18}F]FLT). Targeted application of HSV-1 amplicon vectors containing two therapeutic genes with synergistic antitumor activity (*Escherichia coli* cytosine deaminase, *cd*, and mutated HSV-1 thymidine kinase, *tk39*, fused to green fluorescent protein gene, *gfp*) leads to an overall response rate of 68%, with 18% complete responses and 50% partial responses. Most importantly, we show that the "tissue dose" of HSV-1 amplicon vector–mediated gene expression can be noninvasively assessed by 9-[4-^{18}F-fluoro-3-(hydroxymethyl)butyl]guanine ([^{18}F]FHBG) PET. Therapeutic effects could be monitored by PET with significant differences in [^{18}F]FLT accumulation in all positive control tumors and 72% *in vivo* transduced tumors (P = 0.01) as early as 4 days after prodrug therapy. For all stably and *in vivo* transduced tumors, *cd*IRES*tk39gfp* gene expression as measured by [^{18}F]FHBG-PET correlated with therapeutic efficiency as measured by [^{18}F]FLT-PET. These data indicate that imaging-guided vector application with determination of tissue dose of vector-mediated gene expression and correlation to induced therapeutic effect using multimodal imaging is feasible. This strategy will help in the development of safe and efficient gene therapy protocols for clinical application. [Cancer Res 2007;67(4):1706–15]

Introduction

Gliomas are the most common primary intracranial neoplasms, and ~50% of all gliomas are glioblastomas, the most fatal primary brain neoplasm (1, 2). In view of the high incidence (10–15 per 100,000) and poor prognosis of malignant brain tumors treated with conventional therapies, such as surgery, chemotherapy, brachytherapy, and radiotherapy (3), research focusing on the development of clinically effective alternative therapies such as gene therapy is of utmost importance. Localized transduction of brain tumor cells with therapeutic genes may influence their biological properties by rendering them sensitive to prodrugs, altering the expression of cell cycle regulating proteins, inhibiting angiogenesis, stimulating the immune response, or triggering apoptosis. The helper virus–free herpes simplex virus type 1 (HSV-1) amplicon has been shown to be a safe and efficient vector system in culture and *in vivo* to transduce various central nervous system (CNS)–derived cells including human gliomas (4–8). Clinical studies revealed that a gene therapy approach as an adjuvant to the surgical resection of recurrent high-grade gliomas can be done safely, although clinical responses were observed in only a few patients with small brain tumors (9–14). The lack of therapeutic efficiency of replication-deficient vector systems in clinical settings may be due to insufficient distribution of vector particles throughout the tumor and heterogeneity of tumor tissue with ineffective transduction of proliferating tumor cells. Therefore, further development of clinically valuable gene therapy protocols for use in patients is an important but also a challenging issue, according to experience. To address these challenges, it is important to develop assays that allow (*i*) a noninvasive determination of viable target tissue, which might benefit from a biological treatment paradigm, such as gene therapy, as well as assays (*ii*) for the assessment of the transduced "tissue dose" of a therapeutic gene in patients *in vivo*. Therefore, one important issue for making gene therapy applicable to patients with brain tumors is the establishment of gene therapy protocols, which contain molecular imaging technology including the assessment of endogenous gene expression as marker for viable and proliferating tumor and the noninvasive monitoring of the location, magnitude, and duration of vector-mediated gene expression *in vivo* (7, 15, 16). Previously, we and others have shown the *in vivo* functionality of various gene coexpression constructs based on the internal ribosome entry site (IRES) element serving for the proportional coexpression of a marker gene that can be imaged and a proportionally coexpressed therapeutic gene (7, 17, 18). In the present study, we are using a vector proportionally coexpressing *Escherichia coli* cytosine deaminase (*cd*) as therapeutic gene, HSV-1-*tk39* as positron emission tomography (PET) marker as well as therapeutic gene, and green fluorescent protein gene (*gfp*) fused to HSV-1-*tk39* (19) as cell culture marker gene. The combination of the transgenes *cd* and HSV-1-*tk39*, which encode prodrug-activating enzymes, serves synergistic antitumor activity (20). We show that (*i*) identification of target tissue, (*ii*) imaging-guided vector application, (*iii*) determination of the tissue dose of vector-mediated gene expression, and (*iv*) correlation to the induced therapeutic effect are feasible.

Note: A.H. Jacobs and M.A. Rueger contributed equally to this work.

Requests for reprints: Andreas H. Jacobs, Laboratory for Gene Therapy and Molecular Imaging, Department of Neurology, University of Cologne, Max Planck Institute for Neurological Research, Gleuelerstraße 50, 50931 Cologne, Germany. Phone: 49-221-4726-310; Fax: 49-221-4726-298; E-mail: Andreas.Jacobs@nf.mpg.de.

©2007 American Association for Cancer Research.

doi:10.1158/0008-5472.CAN-06-2418

Downloaded from http://aacrjournals.org/cancerres/article-pdf/67/4/1706/2578556/1706.pdf by guest on 09 December 2023

Materials and Methods

Cells. Rat F98 and RG2 glioma cells, human Gli36dEGFR glioma cells (kind gift of Dr. David Louis, Molecular Neuro-Oncology Laboratory, Massachusetts General Hospital, Boston, MA), and human U87dEGFR glioma cells (kind gift of Dr. H-J. Su Huang, Ludwig Institute for Cancer Research, San Diego, CA) were grown as monolayers in DMEM (Life Technologies, Karlsruhe, Germany) supplemented with 10% fetal bovine serum (Roche Diagnostics, Mannheim, Germany) and 100 units/mL penicillin and 100 μg/mL streptomycin (Life Technologies) at 37°C in a 5% CO_2/95% air atmosphere.

HSV-1 amplicon vector. The HSV-1 amplicon backbone pHSV-GN (kind gift of Dr. Xandra Breakefield, Neurogenetics Unit, Massachusetts General Hospital, Boston, MA; refs. 4, 5) was used to create the coexpression cassette containing *cd, tk39*, and *gfp* genes as previously described (7). Amplicon plasmid was packaged helper virus–free as previously described to generate HSV-1-*cd*IRES*tk39gfp* amplicon vector (HSV-CITG; ref. 7). Purified vector stocks were titrated (transducing units per milliliter) on Gli36dEGFR cells by infecting confluent monolayers in 24-well plates (Falcon, Becton Dickinson GmbH, Heidelberg, Germany) and counting GFP-positive cells 24 h after infection (7). Concentrated virus stocks (1×10^8 transducing units/mL) were stored at −80°C for further use.

Transduction of tumor cell lines. To generate positive control tumors, a retroviral vector encoding the CITG coexpression construct was engineered in the pBABE*puro* Moloney murine leukemia virus–based vector backbone (kind gift of Dr. Miguel Sena-Esteves, Neurogenetics Unit,

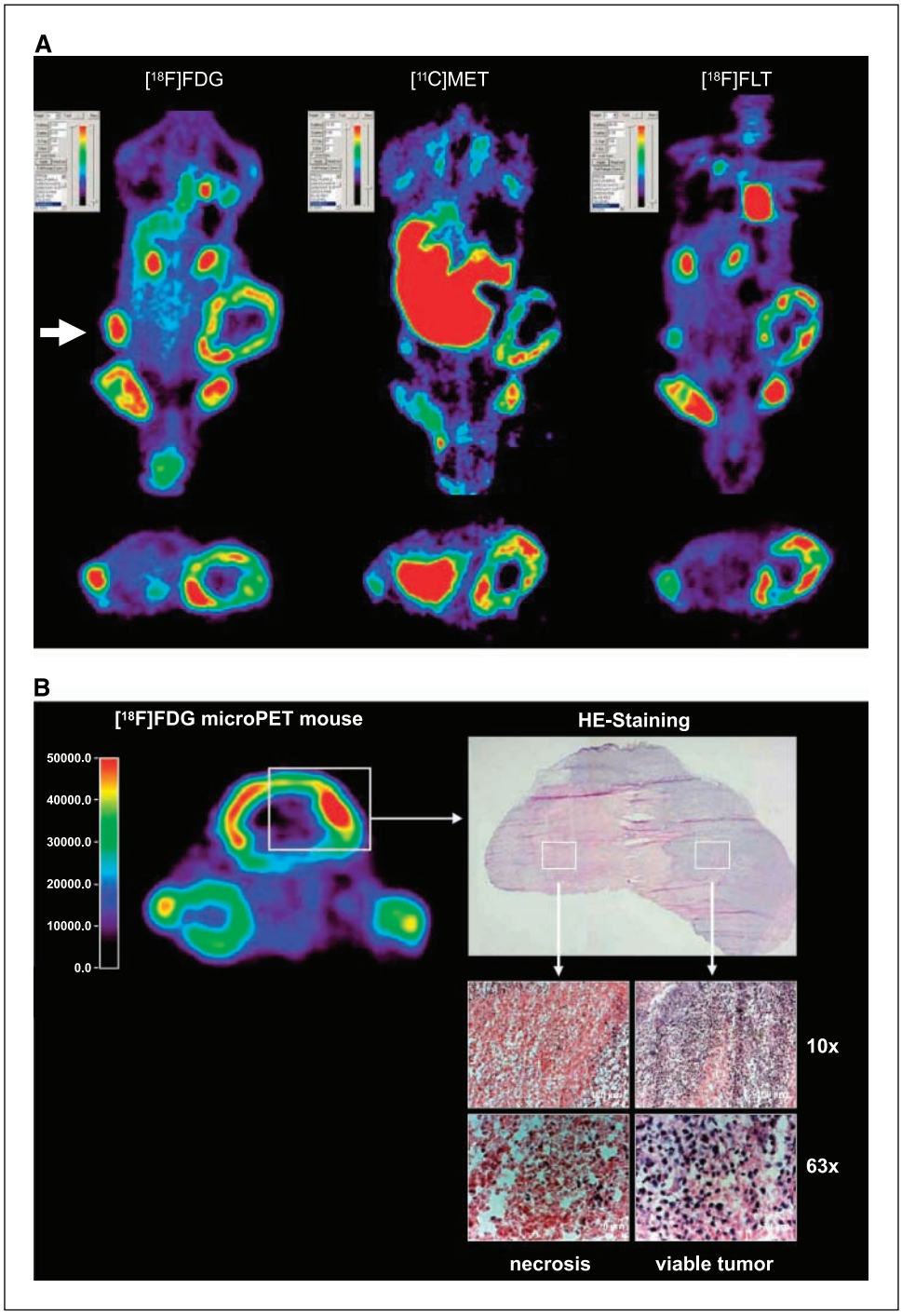

Figure 1. Identification of viable target tissue for gene therapy by multitracer PET in rat (*A*) and mouse (*B*). *A,* whole-body PET from rats harboring four s.c. tumors was obtained with the HRRT scanner enabling imaging of multiple animals at the same time. Acquisition of [^{18}F]FDG-PET, [^{11}C]MET-PET, and [^{18}F]FLT-PET was done on subsequent days. *White arrow,* site of the transaxial slice depicted at the bottom (*A*). In the two small tumors, homogeneous radiotracer uptake is observed. In the medium-sized tumor on the animal's right shoulder, heterogeneous radiotracer uptake is observed. In the large tumor, no radiotracer uptake occurs in the central part of the tumor as indication of necrosis. The whole-body images also clearly depict the mode of excretion of the respective radiotracer: FDG and FLT through kidney and bladder and MET by hepatic metabolization. *Top row,* coronal sections; *bottom row,* transaxial sections. *B,* imaging validation of microPET and histology was done. *Left,* a transaxial section of a [^{18}F]FDG microPET image of a mouse bearing three s.c. gliomas. *Right,* histologic findings of the largest tumor. Tumor tissue with high [^{18}F]FDG accumulation represents viable tissue, whereas lack of tracer accumulation in the central part is identified as necrosis.

Downloaded from http://aacrjournals.org/cancerres/article-pdf/67/4/1706/2578556/1706.pdf by guest on 09 December 2023

Table 1. Radiotracer uptake in viable and necrotic tumor, as well as in various organs, obtained from rats and mice bearing s.c. rat F98 and RG2 gliomas and human Gli36dEGFR and U87dEGFR gliomas

	FDG (ROI/BG)	FLT (ROI/BG)	MET (ROI/BG)	FDG (%ID/g)	FLT (%ID/g)
Tumors					
F98	6.39 ± 3.30 (n = 9)	4.02 ± 2.46 (n = 16)	3.66 ± 1.25 (n = 9)	1.17 ± 0.06 (n = 16)	0.90 ± 0.34 (n = 8)
Rim		1.91 ± 0.49 (n = 2)			0.30 ± 0.17 (n = 2)
Necrosis		0.63 ± 0.05 (n = 2)			-0.12 ± 0.02 (n = 2)
RG2		2.04 ± 0.22 (n = 5)			
Rim	7.98 ± 2.02 (n = 3)		2.59 ± 0.00 (n = 2)		
Necrosis	0.81 ± 0.13 (n = 3)		0.40 ± 0.07 (n = 2)		
U87dEGFR	3.95 ± 1.75 (n = 3)	2.21 ± 0.23 (n = 9)	3.86 ± 0.45 (n = 2)		0.27 ± 0.09 (n = 9)
Gli36dEGFR	2.79 ± 0.81 (n = 18)	2.38 ± 0.40 (n = 3)	2.62 ± 0.15 (n = 4)	1.72 ± 1.11 (n = 6)	
Rim	3.43 ± 0.13 (n = 2)			4.17 ± 0.22 (n = 2)	
Necrosis	1.16 ± 0.29 (n = 2)			0.28 ± 0.50 (n = 2)	
Organs					
Brain	2.88 ± 1.27 (n = 11)	0.30 ± 0.07 (n = 9)	1.29 ± 0.46 (n = 2)	1.24 ± 0.83 (n = 4)	-0.22 ± 0.06 (n = 6)
Kidney	7.21 ± 6.87 (n = 7)	9.97 ± 6.32 (n = 10)	5.35 ± 1.57 (n = 3)		2.90 ± 1.33 (n = 6)
Bladder	37.62 ± 28.55 (n = 10)	20.73 ± 11.31 (n = 9)	8.32 ± 2.75 (n = 3)	10.56 ± 2.17 (n = 3)	13.16 ± 9.40 (n = 6)
Intestine			8.10 ± 1.67 (n = 2)		
Heart	3.29 ± 1.00 (n = 6)				
Liver			12.01 ± 2.70 (n = 6)		
Salivary glands			5.69 ± 1.77 (n = 2)		
Bone			3.26 ± 0.30 (n = 2)		

Abbreviations: ROI, region of interest; BG, background.

Massachusetts General Hospital, Boston, MA) as previously described (7), including an exchange of the puromycin to the neomycin resistance gene. Thereafter, Gli36dEGFR cells were exposed to retrovirus-containing medium in the presence of polybrene (8 μg/mL) for 8 h. GFP-positive Gli36dEGFR-CITG cells were selected under the presence of 1 mg/mL neomycin for 4 weeks. To generate a tumor clone with a defined level of CITG expression, the mixed cell population was sorted by means of fluorescence-activated cell sorting on a FACStar+ (Becton Dickinson). A Gli36dEGFR-CITG clone with high level of GFP expression was propagated for further use.

Animal experiments. All animal procedures were in accordance with the German Laws for Animal Protection and were approved by the local animal care committee and the Bezirksregierung Köln.

Identification and characterization of target tissue by multitracer PET. In a first set of experiments, various glioma cell lines (rat F98 and RG2 glioma, human Gli36dEGFR and U87dEGFR glioma) were implanted s.c. into nude rats (n = 12) and nude mice (n = 8) creating three to four tumors per animal, as previously described (7), to establish the noninvasive identification of target tissue. Tumors were grown to various sizes and multitracer PET imaging [2-^{18}F-fluoro-2-deoxy-D-glucose ([^{18}F]FDG), *methyl*-^{11}C-L-methionine ([^{11}C]MET), or 3′-deoxy-3′-^{18}F-fluoro-L-thymidine ([^{18}F]FLT)] was done to characterize the capability of PET in differentiating viable tumor from necrosis.

Targeted vector application *in vivo*. In a second set of experiments, human Gli36dEGFR glioma cells (5×10^6 in 50 μL of DMEM) were injected s.c. into both flanks of nude mice (n = 22), and retrovirally transduced Gli36dEGFR-CITG cells (5×10^6 in 50 μL of DMEM) were injected s.c. into the neck, resulting in three tumors in each animal. When tumors reached a size of ~0.5 cm^3, HSV-*cd*IRES*tk39gfp* amplicon vectors were injected into one of the two s.c. growing wild-type Gli36dEGFR tumors by direct inoculation with the needle tract following the cranio-caudal axis of the animal (*in vivo* transduced tumor). Three injections were done on subsequent days, achieving a total vector dose of ~2×10^7 transducing units in 200 μL of PBS. In each animal, nontransduced Gli36dEGFR tumors served as negative controls, whereas tumors grown from retrovirally transduced Gli36dEGFR-CITG cells served as positive controls (p.c.). Twenty-four to 48 h after transduction, 9-[4-^{18}F-fluoro-3-(hydroxymethyl)-butyl]guanine ([^{18}F]FHBG) PET imaging was done (see below) with subsequent therapeutic i.p. injection of prodrugs, which were applied daily for 14 days [ganciclovir 25 mg/kg (Cymeven, Hoffmann-La Roche AG, Grenzach-Wyhlen, Germany) and 5-fluorocytosine 500 mg/kg (Ancotil, ICN Pharmaceuticals Germany GmbH, Frankfurt, Germany)].

Volumetry. Tumor sizes were measured twice a week with calipers. For each tumor, a growth curve was fitted and its slope calculated using linear regression analysis. Growth slopes of *in vivo* transduced tumors and of positive control tumors were related to slopes of respective negative controls intraindividually. A ratio between *in vivo* transduced tumor and negative controls of <1 indicated a decelerated growth of transduced tumor and thus a response to therapy. Tumors responding to therapy were further classified as complete responders (tumor disappeared completely) and partial responders (decelerated growth).

Radiosyntheses. [^{18}F]FLT was synthesized according to the method of Machulla et al. (21, 22). In brief, no-carrier-added [^{18}F]FLT was produced by nucleophilic substitution using 2,3′-anhydro-5′-*O*-(4,4′-dimethoxytrityl)-thymidine as precursor with a FLT synthesis module (Nuclear Interface, Muenster, Germany). [^{18}F]Fluoride was produced at the cyclotron (MC 17, Scanditronix, Sweden) via the ^{18}O(p,n)^{18}F reaction by bombardment of >95% enriched [^{18}O]H_2O with 17-MeV protons. The no-carrier-added [^{18}F]fluoride (10–30 GBq) was used for routine. The dry [^{18}F]fluoride ion/K_2CO_3/K2.2.2 was obtained from drying kryptofix 2.2.2 (20 mg, 0.53 mmol) dissolved in 1.5-mL acetonitrile and 20-μL 1 N potassium carbonate. Ten milligrams of precursor dissolved in 0.8-mL DMSO were added to the residue and heated to 160°C for 10 min. The hydrolysis was followed with the addition of 0.3-mL 1 N HCl under 130°C for 5 min. After cooling to 30°C, 0.5-mL 0.5 N Na_2CO_3 was added to the reaction solution, which was first passed through a Sep-Pak cartridge (Al-N) to remove kryptofix 2.2.2 and unreacted fluoride, and the Sep-Pak was washed with 0.5-mL high-performance liquid chromatography solvent (10% ethanol in water). Finally, the effluent was automatically injected onto a semipreparative column [synthesis module: Phenomenex Luna C-18(2) 5 μm, 250 × 10 mm; precolumn: Phenomenex Luna C-18(2) 5 μm, 50 × 10 mm] for high-performance liquid chromatography purification. The no-carrier-added

Downloaded from http://aacrjournals.org/cancerres/article-pdf/67/4/1706/2578556/1706.pdf by guest on 09 December 2023

[^{18}F]FLT (10–40 mCi) was collected using 10% (FLT) ethanol in water as the mobile phase at a flow rate of 5.5 mL/min. [^{18}F]FDG (23), [^{11}C]MET (24), and [^{18}F]FHBG (7) were produced as previously described.

Multimodal imaging. T_1-weighted magnetic resonance images for localization of tumors were obtained in the second set of experimental animals (n = 22 nude mice) on a 1.5-T Philips Gyroscan Intera before *in vivo* transduction. PET imaging was done in all animals from both sets of experiments using either a high-resolution research tomograph (ECAT HRRT, CTI/Siemens PET Systems, Knoxville, TN; 207 image planes; spatial resolution of 2.0-mm full width at the half maximum at the center of the field of view) or a microPET (Concorde Microsystems, Inc., Knoxville, TN; 63 image planes; 2.0-mm full width at the half maximum). Radiotracer was administered i.v. (tail vein) into experimental animals with the following doses: no-carrier-added [^{18}F]FDG, 200 μCi/mouse, 400 μCi/rat; no-carrier-added [^{11}C]MET, 400 μCi/mouse, 800 μCi/rat; no-carrier-added [^{18}F]FLT, 250 μCi/mouse, 500 μCi/rat; no-carrier-added [^{18}F]FHBG, 300 μCi/mouse. Emission scans (duration, 30 min) were obtained starting at 40 min ([^{18}F]FDG), 20 min ([^{11}C]MET), 30 min ([^{18}F]FLT), 20 to 120 min (early), and >120 min (late; [^{18}F]FHBG) after tracer application. Maximum a posteriori reconstruction of microPET images was done without scatter and attenuation correction. For quantification of images, a reference standard sample of radiotracer was

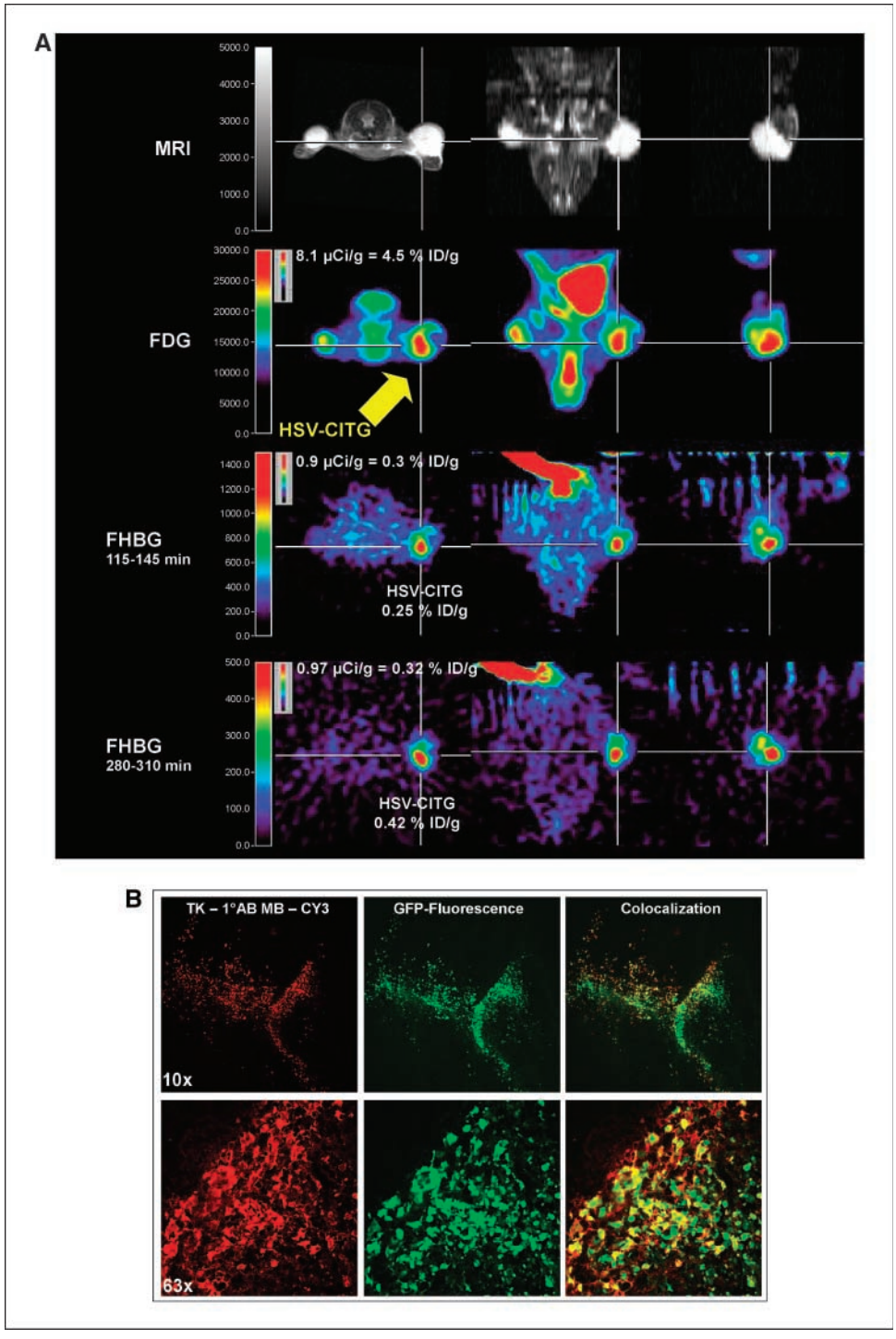

Figure 2. Multimodal imaging and image validation. *A,* experimental protocol for identification of viable target tissue and assessment of vector-mediated gene expression *in vivo* in a mouse model with three s.c. gliomas. *Row 1,* localization of tumors is displayed by MRI. *Row 2,* the viable target tissue is displayed by [^{18}F]FDG-PET; note the signs of necrosis in the lateral portion of the left-sided tumor (*arrow*). *Rows 3* and *4,* following vector application into the medial viable portion of the tumor (*arrow*), the tissue dose of vector-mediated gene expression is quantified by [^{18}F]FHBG-PET. *Row 3,* an image acquired early after tracer injection, which is used for coregistration; *row 4,* a late image with specific tracer accumulation in the tumor that is used for quantification. *B,* good colocalization of the expression of both genetic components of the *tkgfp* fusion construct by thymidine kinase immunohistochemistry and GFP fluorescence microscopy in a tumor that had been injected with *tkgfp*-expressing HSV-1 amplicon vectors and imaged by [^{18}F]FHBG-PET.

Downloaded from http://aacrjournals.org/cancerres/article-pdf/67/4/1706/2578556/1706.pdf by guest on 09 December 2023

placed within the field of view of the PET scanner. To allow image coregistration, a newly developed software was used allowing for fast automated coregistration of multimodal imaging data as previously described (VINCI; ref. 25). Data evaluation was based on a region of interest analysis of PET images to determine maximal radioactivity concentrations within tumors. After background (mediastinum) subtraction, data were decay corrected and divided by the total injected dose to represent percentage injected dose per gram (%ID/g).

As gene therapy vectors have to be applied into viable tumor tissue to ensure expression of therapeutic genes, a protocol for acquisition of a series of multimodal images was established, which allows identification of viable target tissue before the initiation of gene therapy using [^{18}F]FDG-PET, [^{11}C]MET-PET, or [^{18}F]FLT-PET. The respective images were coregistered to magnetic resonance images and used for targeted vector application. Following the injection of HSV-1-*cd*IRES*tk39gfp* amplicons, vector-mediated gene expression *in vivo* was analyzed by the use of the PET-marker gene *tk39* and its specific tracer [^{18}F]FHBG (26, 27). [^{18}F]FHBG-PET images acquired early after tracer injection was used for coregistration with the other imaging modalities due to high background of untrapped [^{18}F]FHBG. Repeat imaging later than 120 min after [^{18}F]FHBG injection was used to evaluate specific [^{18}F]FHBG accumulation in transduced tumor portions to ensure quantification of the tissue dose of vector-mediated gene expression (in %ID/g). Moreover, [^{18}F]FLT-PET was done as baseline evaluation before *in vivo* transduction and as therapy monitoring after 1 week of therapy. Therapeutic efficiency was quantified by the difference of [^{18}F]FLT accumulation (in %ID/g) before and after therapy (ΔFLT).

Tissue sampling and histology. After the last PET measurements, animals were killed and s.c. tumors were extracted rapidly. After fixation (4% paraformaldehyde, 4°C, 24 h), tumors were embedded in tissue-freezing medium (Jung, Nussloch, Germany) and 20-μm frozen sections were prepared along the transaxial plane relative to the tumor position in the animal. H&E staining on the tissue was done according to standard protocols. Image validation on tumor tissue sections, which has been transduced by *tkgfp*-expressing HSV-1 amplicon vectors, has been done as previously described (7, 28).

Statistics. Descriptive statistics and regression analysis were done with Microsoft Excel 2002 (Microsoft Corp., Redmond, WA). Student's *t* test was done with SigmaStat 3.0 (SPSS, Inc., Chicago, IL); statistical significance was set at $P < 0.05$.

Results

Identification of target tissue for gene therapy is possible by multitracer PET. To validate the feasibility of PET for the identification of viable target tissue, which would be amenable for the local application of gene therapy vectors, in the first set of experiments, tumors growing s.c. in nude rats ($n = 12$) and nude mice ($n = 8$) were visualized by multitracer PET and assessed with respect to the different characteristics of radiotracer uptake within the tumor. Three radiotracers were used, of which two have routine clinical application in patients with gliomas ([^{18}F]FDG and [^{11}C]MET) and one is known to assess tumor proliferation ([^{18}F]FLT). [^{18}F]FDG as a surrogate marker for cellular density, [^{11}C]MET as a surrogate marker for neovascularization, and [^{18}F]FLT as a surrogate marker for proliferative activity displayed homogeneous uptake in small tumors and heterogeneous uptake in larger tumors (Fig. 1*A*). In the latter, no radiotracer uptake occurred in the central part of the tumors indicative of central necrosis. For image validation, transaxial PET images were coregistered with histology showing a correlation between the lack of tracer accumulation and the histologic signs of necrosis, whereas positive tracer accumulation correlated with viable tumor tissue (Fig. 1*B*). Radiotracer distribution in viable tumor tissue and necrosis for the different tumor types and in various organs are depicted in Table 1. Tumor-to-background ratios ranged from 1.9 to 8.0 in viable tumor tissue and from 0.4 to 1.2 in necrosis. As an indication of the mode of excretion, [^{18}F]FDG and [^{18}F]FLT showed substantial uptake in kidney and bladder, and [^{11}C]MET accumulation was highest in the liver (Fig. 1*A*).

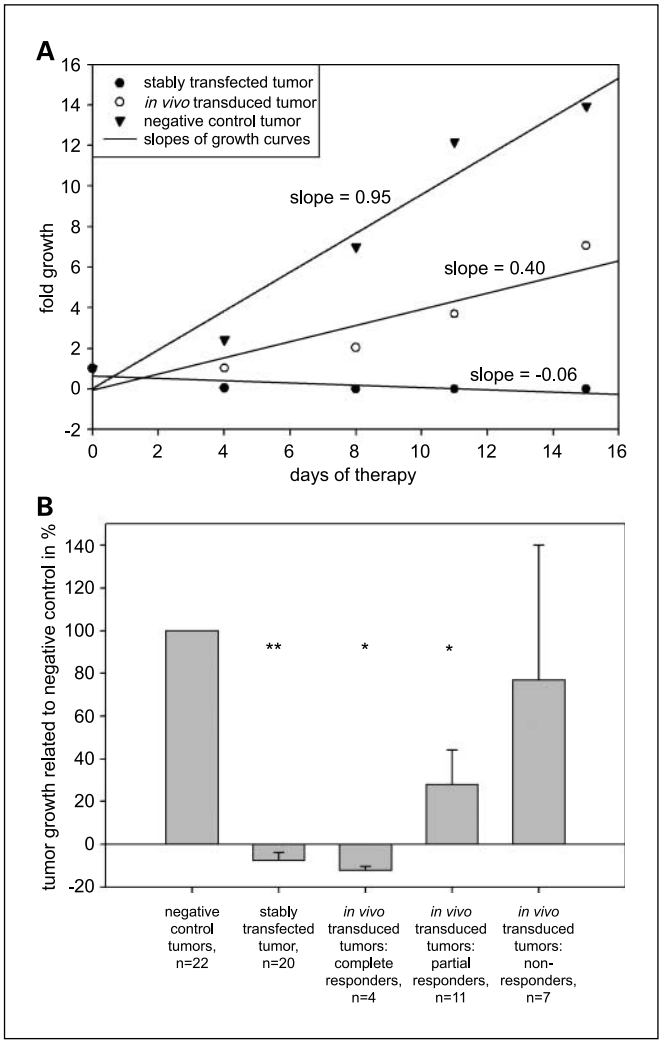

Figure 3. Response to gene therapy as measured by tumor volumes. *A,* an example of tumor growth under therapy for one representative mouse. Growth slopes were calculated by linear regression analysis. Growth slope of *in vivo* transduced tumor (0.40) is smaller than that of negative control tumor (0.95), indicating partial response to therapy. The positive control tumor showed complete response to therapy and disappeared (slope −0.06). *B,* volumetric data of tumor growth under therapy are displayed for all experimental animals ($n = 22$). Classification of *in vivo* transduced tumors as complete responders, partial responders, and nonresponders according to growth slopes. *Columns,* mean growth slopes given as percentage of negative control tumors; *bars,* SD. Stably transfected tumors, as well as *in vivo* transduced and responding tumors, showed significantly decelerated growth related to negative control tumors (*, $P < 0.05$; **, $P < 0.01$).

Imaging-guided vector application is feasible. To enable targeted application of vector particles into viable tumor tissue, image-guided vector application was done as depicted in Fig. 2*A* with (*i*) magnetic resonance imaging (MRI) for localization of tumor; (*ii*) [^{18}F]FDG-PET for identification of viable target tissue; (*iii*) early [^{18}F]FHBG-PET for coregistration; and (*iv*) late [^{18}F]FHBG-PET for determination of the total tissue dose of vector-mediated gene expression. Mean cdIREStk39gfp expression, as measured by [^{18}F]FHBG accumulation, was 1.22 ± 0.83% ID/g for stably transfected positive control tumors and mean transduction efficiency

Downloaded from http://aacrjournals.org/cancerres/article-pdf/67/4/1706/2578556/1706.pdf by guest on 09 December 2023

of *in vivo* transduced tumors was 0.37 ± 0.30% ID/g. For image validation, thymidine kinase immunohistochemistry and GFP fluorescence microscopy have been done on tumors that had been imaged by [^{18}F]FHBG-PET after transduction with *tkgfp*-expressing HSV-1 amplicon vectors showing colocalization of both components of the *tkgfp* fusion construct (Fig. 2*B*).

The outcome as measured by tumor volume showed 50% partial and 18% complete responses. To assess the gene therapeutic effect by standard volumetric assay, 22 nude mice with human Gli36dEGFR gliomas were transduced *in vivo* with HSV-1-*cd*IRES*tk39gfp* amplicon vectors and subjected to prodrug therapy with ganciclovir and 5-fluorocytosine. Growth slopes of tumors were determined and used to assess response to therapy (Fig. 3*A*). All 22 positive control tumors stably expressing *cd* and *tk39gfp* were successfully treated with prodrugs leading to disappearance of tumors within 10 days (Fig. 3*B*). Of 22 *in vivo* transduced tumors, 4 tumors disappeared completely during prodrug therapy (complete responders). Eleven other *in vivo* transduced tumors showed a decelerated growth compared with the negative control tumors in the respective same animals (partial responders, growth of 28 ± 16% compared with negative controls). This represents a response rate of 15 of 22 (68%) *in vivo* transduced tumors (Fig. 3*B*). Growth slopes of tumors responding to gene therapy differed significantly from those of negative control tumors (*t* test, $P < 0.05$). Seven of 22 *in vivo* transduced tumors did not respond to prodrug therapy.

[^{18}F]FLT-PET is able to assess tumor response after 1 week of prodrug therapy. To assess the effects of gene therapy on tumor proliferation, [^{18}F]FLT-PET was done before and after therapy to monitor response to therapy with regard to proliferative

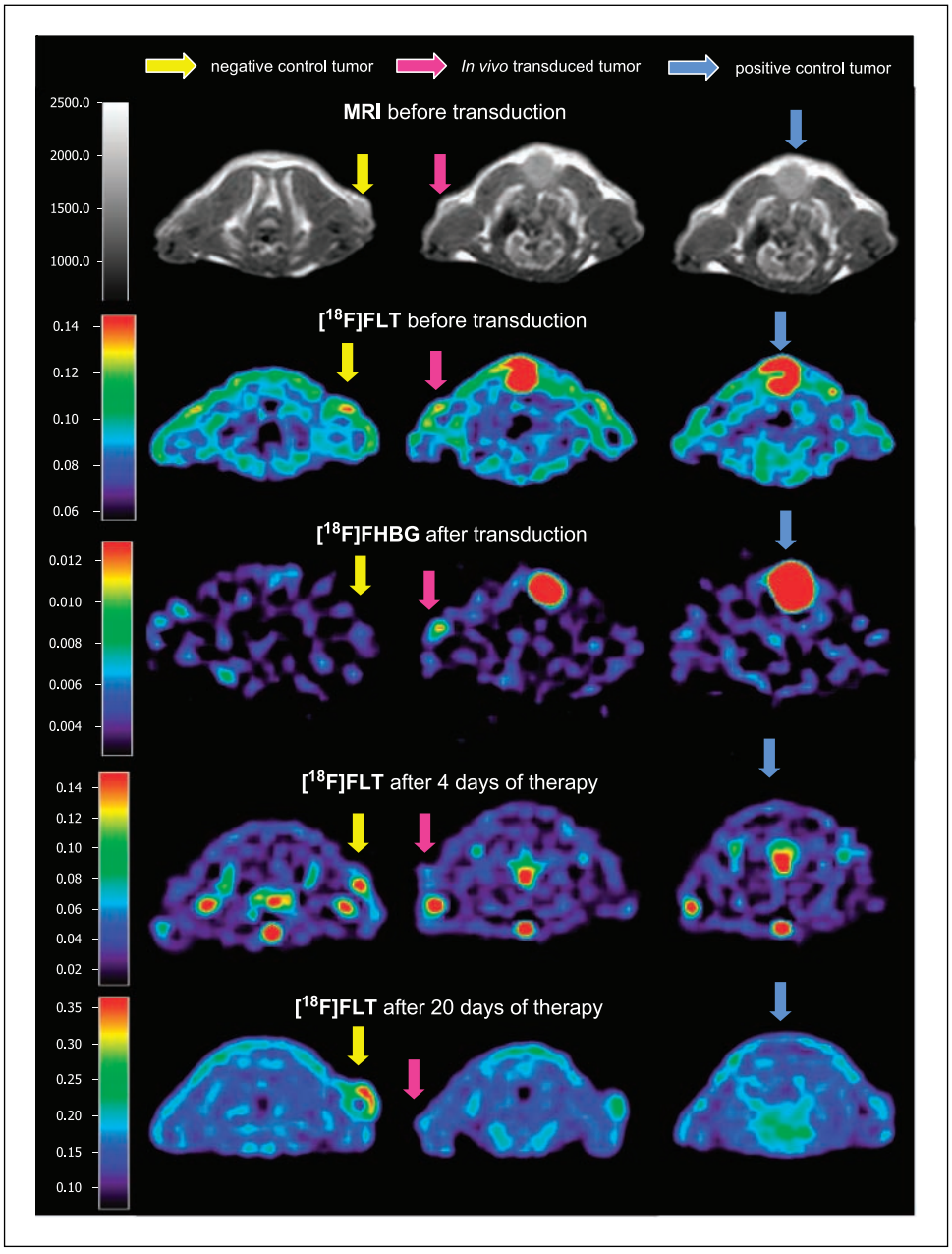

Figure 4. Protocol for imaging-guided gene therapy using MRI, [^{18}F]FLT-PET, and [^{18}F]FHBG-PET. Row 1 (MRI) and row 2 ([^{18}F]FLT-PET) display tumor morphology and proliferative activity before therapy; row 3 ([^{18}F]FHBG-PET) illustrates the intensity of exogenous gene expression after *in vivo* transduction; and rows 4 and 5 show early and late [^{18}F]FLT-PET follow-up under therapy. The negative control tumor shows no expression of HSV-1-*tk* and an increase in size and proliferative activity in the course of therapy; the *in vivo* transduced tumor with a distinct *tk* expression in [^{18}F]FHBG-PET, as well as the positive control tumor, disappears under therapy.

Downloaded from http://aacrjournals.org/cancerres/article-pdf/67/4/1706/2578556/1706.pdf by guest on 09 December 2023

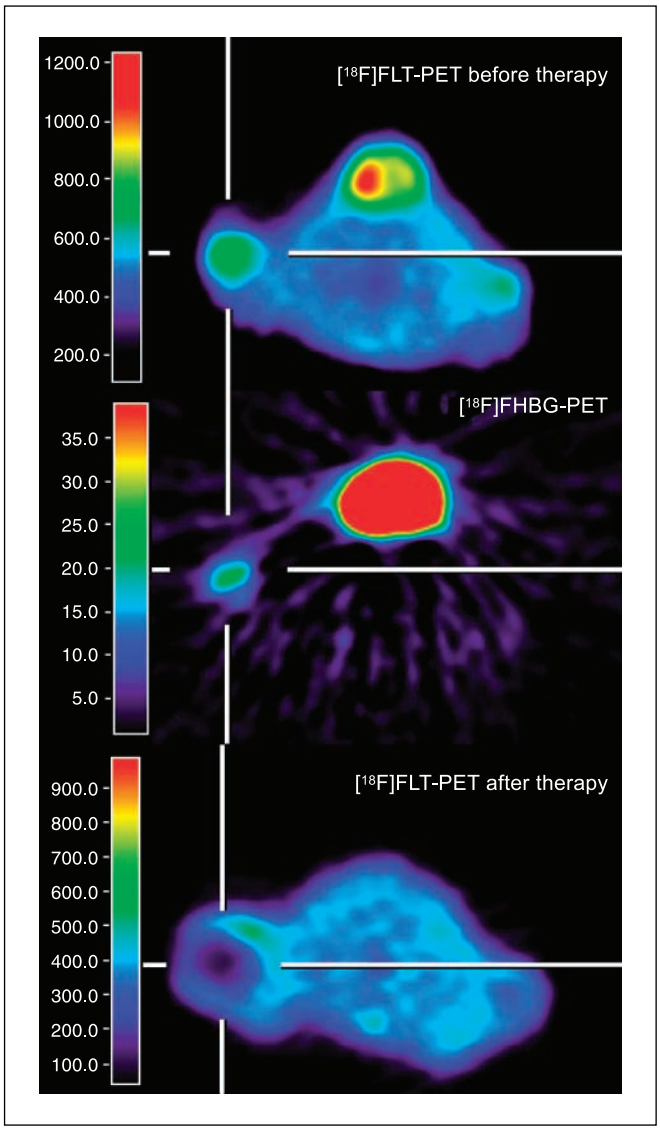

Figure 5. Response to gene therapy of an *in vivo* transduced tumor (*cross marker*) and a positive control tumor (*neck*) as imaged by [^{18}F]FLT-PET. [^{18}F]FLT-PET after administration of prodrugs shows a circumscribed area lacking radiotracer uptake colocalizing to the transduced portion of the tumor as visualized by [^{18}F]FHBG-PET. At the same time, the positive control tumor disappeared.

activity. Due to the complexity of the protocol, the complete series of MRI and PET studies as depicted in Fig. 4 could be obtained in 11 of 22 (50%) animals only. Significant differences in [^{18}F]FLT accumulation before (3.38 $\pm$ 3.65% ID/g) and after therapy (0.06 $\pm$ 0.19% ID/g; paired t test, P = 0.01) were obtained in all stably cdIREStk39gfp expressing positive control tumors (Figs. 4–6). Eight of 11 *in vivo* transduced tumors responded to gene therapy as visualized by [^{18}F]FLT-PET, showing a significant decrease in [^{18}F]FLT accumulation after therapy (1.91 $\pm$ 1.12 versus 0.42 $\pm$ 1.31% ID/g; paired t test, $P < 0.01$; Figs. 4–6*A*). Three of 11 *in vivo* transduced tumors did not respond to therapy as measured by [^{18}F]FLT-PET (Fig. 6*A*). For all stably transfected and *in vivo* transduced tumors, the level of cdIREStk39gfp expression as measured by [^{18}F]FHBG-PET correlated with the resulting therapeutic efficiency as measured by the difference of [^{18}F]FLT accumulation before and after therapy (R = 0.73; $P < 0.01$; Fig. 6*B*). For all tumors, volumetric data did not correspond directly to [^{18}F]FLT-PET and [^{18}F]FHBG-PET as some tumors showed a partial response, as indicated by [^{18}F]FLT-PET, with no reduction in overall tumor volume (Figs. 5 and 6*C*). A positive correlation (R = 0.83) was found between volumetric data and [^{18}F]FLT-PET in the subsets of tumors that responded to therapy as complete responders (Fig. 6*C*). Figure 6*C* also indicates a positive relation between the change in FLT uptake and volumetry in nonresponding tumors (R = 0.57). It should be pointed out that 22 mice have been studied in the same study protocol. Volumetric data were obtained in all animals; the full set of imaging data could only be obtained in 11 of these 22 animals. The correlations between FLT-PET and FHBG-PET (Fig. 6*B*), as well as between FLT-PET and volumetry (Fig. 6*C*), are based on these 11 animals.

Discussion

Gene therapy is one of the promising approaches for a targeted treatment of tumors. However, its efficiency in clinical application for patients with glioblastomas has been disappointing thus far and reported to occur only in small tumors. The most important hurdles for successful application of gene therapy in patients with glioblastomas are the heterogeneity of tumor tissue and the limited transduction efficiency of current vectors. In this study, we therefore aimed at the further characterization of these two limiting factors by (*i*) identification of viable target tissue that might benefit from gene therapy and (*ii*) quantification of the transduction efficiency, both assessed noninvasively by PET. The imaging protocol used was aimed to reflect the procedures that would be done in a clinical situation. First, MRI was used for exact tumor localization. Then, markers for endogenous gene expression, such as FDG and FLT for the expression of glucose and nucleoside transporters, as well as for the expression of cellular hexokinase and thymidine kinase genes, respectively, and MET for the expression of amino acid transporters, were used to identify the actively proliferating tumor tissue. In addition, these tracers can be used as surrogate markers for cellular density (FDG), neovascularization (MET), and proliferative activity (FLT). FLT was also used to determine the gene therapy–induced inhibition of proliferative activity of the tumor. A marker for exogenously introduced therapeutic gene expression (FHBG) could localize the transduced tissue dose of therapeutic gene expression. Using this "imaging-guided" gene therapy protocol, we found a response rate of 68% of the *in vivo* transduced tumors with 18% complete responders as deduced from tumor volumetry. Most importantly, the primary transduction efficiency as measured by FHBG-PET could be correlated with the induced therapeutic effect, although follow-up imaging data by use of FLT-PET could only be obtained in 50% of investigated animals due to the complexity of the protocol. In tumors that responded to therapy, the decrease in FLT uptake corresponded to the decrease in tumor volume.

Several clinical gene therapy trials have outlined the promises as well as the difficulties associated with gene therapy. Suicide gene therapy for patients with recurrent glioblastoma using the HSV-1-TK/ganciclovir system has been done using retroviral (11, 14), adenoviral (29, 30), and HSV-1 (10, 13) vectors. Usually, imaging follow-up in those studies is done by gadolinium-enhanced MRI bearing the difficulty of assessing residual active tumor tissue after therapy and differentiating it from treatment-induced enhancement. Overall, it has been shown that suicide gene therapy has

Downloaded from http://aacrjournals.org/cancerres/article-pdf/67/4/1706/2578556/1706.pdf by guest on 09 December 2023

potential therapeutic efficacy, which nevertheless remains either partial or occurs only in single patients with small tumors. Explanations for the limited therapeutic efficiency include the heterogeneity of target tissue (31), insufficient transduction efficiency (32), and interindividual variability of infectivity by vector particles due to different entry receptor status (8). Ongoing research focuses on the development of safe replication-conditional vectors and genetic approaches to target vascular and growth factor receptors and transforming growth factor-β, as well as to stimulate the immune response. All of these approaches rely on the noninvasive visualization of the target to allow an efficient targeted application of vectors and therapeutic genetic material and to allow a direct assessment of efficiency (15).

Some authors have reported noninvasive imaging follow-up of suicide gene therapy in experimental models, but these studies were usually done on tumors grown from stably transfected cell lines (33–36). Few studies used molecular imaging–guided follow-up after transduction of therapeutic genes *in vivo* using adenoviral (37, 38) and lentiviral vectors (39). To our knowledge, this is the first study of a HSV-1 amplicon vector–mediated gene therapy approach that uses multimodal molecular imaging techniques for noninvasive follow-up in a glioma model.

HSV-1 has many properties that make it especially suitable as a vector to treat diseases affecting the CNS (i.e., its natural neurotropism, high transduction efficiency, large transgene capacity, and the ability of entering a latent state in neurons). Besides replication-conditional HSV-1 mutants, the "gutless" HSV-1 amplicon vector has several properties, which make it a promising candidate gene transfer vehicle for clinical use (6, 40). No virus proteins are encoded; it is nearly nontoxic when packaged without contaminating helper virus; and it can infect most mammalian cell types and can accommodate large fragments of foreign DNA. Helper virus–free packaging systems use replication-competent, packaging-defective genomes of HSV-1 to provide the functions necessary for replication and packaging of cotransfected amplicon DNA (5, 41, 42). The resulting stocks of helper virus–free HSV-1 amplicons have been shown to be safe and efficient in culture and *in vivo*, and they transduce a variety of CNS-derived cells including human gliomas (4, 6, 7, 43, 44). Moreover, we have shown that vector-mediated gene expression mediated by replication-conditional and HSV-1 amplicon vectors can be noninvasively assessed *in vivo* by PET (7, 28).

Noninvasive localization of exogenously introduced gene expression by PET relies on the transduction of "marker genes" along with the therapeutic genes. Radiolabeled 9-(4-^{18}F-fluoro-3-hydroxymethylbutyl)guanine ([^{18}F]FHBG) is a safe and efficient PET tracer to detect HSV-1-*tk* expression (26, 45). Mutant HSV-1 thymidine kinases have been developed that, compared with wild-type thymidine kinase, render cells more sensitive to specific nucleoside analogues like the prodrug ganciclovir used for therapy and the PET tracer [^{18}F]FHBG used for imaging. We therefore used the

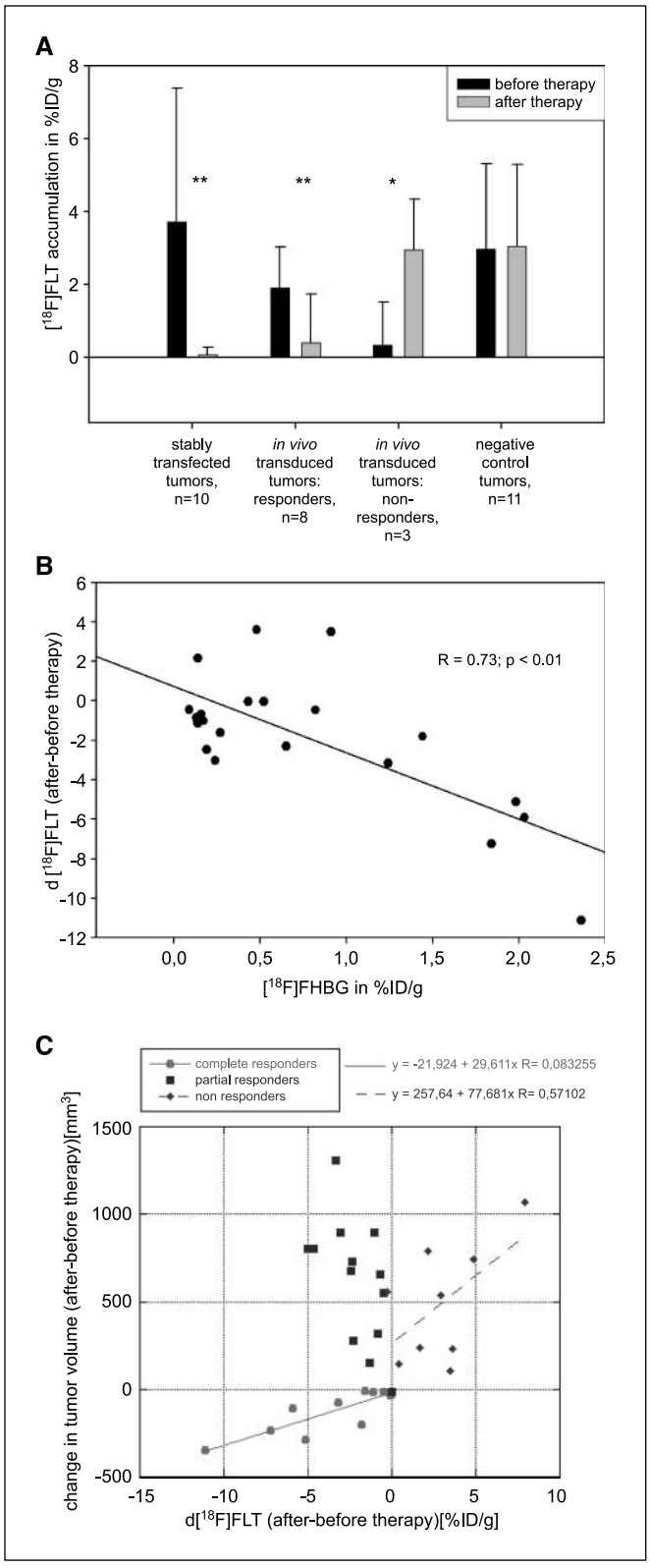

Figure 6. Response to therapy as assessed by [^{18}F]FLT-PET. *A,* [^{18}F]FLT accumulation (in %ID/g) after therapy compared with baseline accumulation is significantly decreased in stably transfected tumors. Eight of 11 *in vivo* transduced tumors showed a significant decrease in [^{18}F]FLT accumulation after therapy (*, $P < 0.05$; **, $P < 0.01$). *Bars,* SD. *B,* correlation between the intensity of cdIREStk39gfp expression, which is equivalent to transduction efficiency, and tissue dose of vector-mediated therapeutic gene expression, as measured by [^{18}F]FHBG-PET (in %ID/g), and the induced therapeutic effect as measured by [^{18}F]FLT-PET ($R = 0.73$, $P < 0.01$). Therapeutic effect (Δ[^{18}F]FLT) was calculated as the difference between [^{18}F]FLT accumulation after and before therapy. *C,* relation between changes in volumetry and FLT uptake. Changes in tumor volume and FLT uptake were plotted for all tumors grown in 11 animals where the full imaging protocol could be completed. There is a strong correlation between volumetry and change in FLT uptake ($R = 0.83$) for those tumors responding to therapy (complete responders) and a weaker correlation ($R = 0.57$) for those tumors not responding to therapy (nonresponders). No correlation was found for those tumors where focal alterations of FLT uptake occurred, which did not lead to a reduction in overall tumor volume (partial responders).

Downloaded from http://aacrjournals.org/cancerres/article-pdf/67/4/1706/2578556/1706.pdf by guest on 09 December 2023

mutated thymidine kinase HSV-1-*tk39* (7, 46) to serve as a PET marker gene and as a therapeutic gene at the same time.

To enhance the antitumoral effects of our construct, we used two therapeutic genes, *Escherichia coli cd* and HSV-1-*tk39*, which confer sensitivity to the prodrugs 5-fluorocytosine and ganciclovir, respectively. TK39 phosphorylates the nontoxic prodrug ganciclovir, which then becomes phosphorylated by endogenous kinases to ganciclovir-triphosphate, causing chain termination and single-strand breaks on incorporation into DNA (47). Moreover, not only cells expressing the transgene but also neighboring nontransduced tumor cells can undergo cell death by bystander killing (48). CD deaminates the nontoxic pyrimidine 5-fluorocytosine to the cytotoxic 5-fluorouracil (5-FU). 5-FU is processed both to the ribonucleotide 5-fluorouracil triphosphate, which is incorporated into RNA and interferes with RNA processing, and to 5-fluoro-2-deoxyuridine-5-monophosphate, which irreversibly inhibits thymidylate synthase and interferes with DNA synthesis (49). TK/ganciclovir– and CD/5-fluorocytosine–induced apoptoses converge at a mitochondrial pathway triggered by different mechanisms of modulation of Bcl-2 proteins (50). The combination of those two therapeutic genes has been shown to have synergistic effects in glioma cells (20, 51, 52), although Moriuchi et al. (53) critically proposed a mutual counteractivity. Previously, we have shown for our *cd*IRES*tk39gfp* construct a proportional coexpression of *cd* and *tk39gfp* and did not observe an attenuation of the killing of glioma cells for this combination (7).

To localize and distinguish the viable tissue of the tumors and to observe their response to therapy, the clinical PET marker for tumor proliferation, [^{18}F]FLT, was used. [^{18}F]FLT has recently been introduced as a PET tracer for tumor imaging (54–56). 3′-Deoxy-3′-fluorothymidine (FLT) is a nucleoside analogue and is phosphorylated to 3′-fluorothymidine monophosphate (FLT-MP) through the S phase–specific enzyme TK-1. Phosphorylation of FLT accurately reflects changes in TK-1 enzyme activity (57). This phosphorylation leads to an intracellular trapping of FLT-MP, which is a prerequisite for its use as a PET tracer. The [^{18}F]FLT uptake has been shown to correlate to proliferation *in vivo* as measured by Ki67 proliferation index (58). Besides its application for various other tumor types, [^{18}F]FLT-PET has also recently proved useful for evaluating tumor grade and cellular proliferation in brain tumors (59–61). [^{18}F]FLT is especially suitable for therapy follow-up, as it reflects early effects of anticancer therapy (62). In tumors that responded to gene therapy, we found [^{18}F]FLT accumulation to decrease already within a few days after initiation of prodrug application (Figs. 4–6). A corresponding reduction in tumor volume was found (Fig. 6*C*). It should be pointed out that [^{18}F]FLT-PET revealed additional, complementary information about tumor progression than volumetry. Some tumors that increased in volume during the course of treatment showed decreasing proliferation as measured by [^{18}F]FLT accumulation in follow-up studies. This decreased proliferative activity was always observed in the part of the glioma where *in vivo* transduction had taken place, which was visualized as HSV-1-*tk39* expression by [^{18}F]FHBG-PET, whereas the rim of the tumor usually showed a higher proliferative activity (Fig. 5). Quantification of [^{18}F]FLT accumulation was done in the same area where *in vivo* transduction has been observed by [^{18}F]FHBG-PET. A prerequisite for this was the exact coregistration of [^{18}F]FHBG-PET and [^{18}F]FLT-PET images using a newly in-house developed software for fast coregistration of multimodal image data sets (VINCI; ref. 25). Because we used a replication-deficient amplicon vector that could transduce tumor cells only at the injection site, the therapeutic response in larger tumors was therefore restricted to that injection site also. Thus, the transduced therapeutic gene caused a local regression of tumor proliferation, which was not sufficient to stop proliferation of the entire tumor. These findings are supported by the correlation between level of CD-IRES-TK39-GFP expression as measured by [^{18}F]FHBG-PET and therapeutic efficiency as measured by [^{18}F]FLT-PET (Fig. 6*B*).

In summary, we conclude that the identification of target tissue enables targeted vector application, which will be an essential tool in clinical applications. Determination of the tissue dose of vector-mediated gene expression is feasible and enables a correlation to the induced therapeutic effect. This type of multimodal imaging protocol, together with improved vector and promoter technology (63, 64) for tumor-specific targeting, will be of great importance for the further development of clinical gene therapy trials, as an ineffective transduction and low tissue dose of therapeutic gene can be noted early, which may guide the further management of the patient to avoid that he is treated in vain. This type of imaging-guided gene therapy protocol will therefore facilitate the development of safe and efficient gene therapy protocols for clinical application.

Acknowledgments

Received 7/3/2006; revised 9/12/2006; accepted 10/23/2006.

Grant support: Deutsche Forschungsgemeinschaft (DFG-Ja98/1-2), Ministerium für Schule, Wissenschaft und Forschung NRW (MSWF 516-40000299), Center for Molecular Medicine Cologne (CMMC-TV46), and 6th FW EU grant EMIL (LSHC-CT-2004-503569).

The costs of publication of this article were defrayed in part by the payment of page charges. This article must therefore be hereby marked *advertisement* in accordance with 18 U.S.C. Section 1734 solely to indicate this fact.

Downloaded from http://aacrjournals.org/cancerres/article-pdf/67/4/1706/2578556/1706.pdf by guest on 09 December 2023

References

1. Kleihues P, Cavenee WK, editors. Pathology and genetics of tumours of the nervous system (WHO). Lyon: IARC Press; 2000.
2. Preston-Martin S. Epidemiology. In: Berger MS, Wilson CD, editors. The gliomas. Philadelphia (PA): Saunders; 1999. p. 2–11.
3. Tatter SB, Harsh GR. Current treatment modalities for brain tumor. In: Chiocca EA, Breakefield XO, editors. Gene therapy for neurological disorders and brain tumors. Totowa (NJ): Humana Press; 1998. p. 161–89.
4. Aboody-Guterman KS, Pechan PA, Rainov NG, et al. Green fluorescent protein as a reporter for retrovirus and helper virus-free HSV-1 amplicon vector-mediated gene transfer into neural cells in culture and *in vivo*. Neuroreport 1997;8:3801–8.
5. Fraefel C, Song S, Lim F, et al. Helper virus-free transfer of herpes simplex virus type 1 plasmid vectors into neural cells. J Virol 1996;70:7190–7.
6. Jacobs A, Breakefield XO, Fraefel C. HSV-1-based vectors for gene therapy of neurological diseases and brain tumors. Part II. Vector systems and applications. Neoplasia 1999;1:402–16.
7. Jacobs A, Winkeler A, Hartung M, et al. Improved herpes simplex virus type 1 amplicon vectors for proportional coexpression of positron emission tomography marker and therapeutic genes. Hum Gene Ther 2003;14:277–97.
8. Rueger MA, Winkeler A, Miletic H, et al. Variability in infectivity of primary cell cultures of human brain tumors with HSV-1 amplicon vectors. Gene Ther 2005; 12:588–96.
9. Klatzmann D, Valery CA, Bensimon G, et al. A phase I/II study of herpes simplex virus type 1 thymidine kinase "suicide" gene therapy for recurrent glioblastoma. Study Group on Gene Therapy for Glioblastoma. Hum Gene Ther 1998;9:2595–604.
10. Markert JM, Medlock MD, Rabkin SD, et al. Conditionally replicating herpes simplex virus mutant, G207 for the treatment of malignant glioma: results of a phase I trial. Gene Ther 2000;7:867–74.
11. Rainov NG. A phase III clinical evaluation of herpes simplex virus type 1 thymidine kinase and ganciclovir gene therapy as an adjuvant to surgical resection and

radiation in adults with previously untreated glioblastoma multiforme. Hum Gene Ther 2000;11:2389–401.
12. Ram Z, Culver KW, Oshiro EM, et al. Therapy of malignant brain tumors by intratumoral implantation of retroviral vector-producing cells. Nat Med 1997;3:1354–61.
13. Rampling R, Cruickshank G, Papanastassiou V, et al. Toxicity evaluation of replication-competent herpes simplex virus (ICP 34.5 null mutant 1716) in patients with recurrent malignant glioma. Gene Ther 2000;7:859–66.
14. Shand N, Weber F, Mariani L, et al. A phase 1-2 clinical trial of gene therapy for recurrent glioblastoma multiforme by tumor transduction with the herpes simplex thymidine kinase gene followed by ganciclovir. GLI328 European-Canadian Study Group. Hum Gene Ther 1999;10:2325–35.
15. Jacobs A, Voges J, Reszka R, et al. Positron-emission tomography of vector-mediated gene expression in gene therapy for gliomas. Lancet 2001;358:727–9.
16. Tjuvajev JG, Stockhammer G, Desai R, et al. Imaging the expression of transfected genes *in vivo*. Cancer Res 1995;55:6126–32.
17. Tjuvajev JG, Joshi A, Callegari J, et al. A general approach to the non-invasive imaging of transgenes using *cis*-linked herpes simplex virus thymidine kinase. Neoplasia 1999;1:315–20.
18. Yu Y, Annala AJ, Barrio JR, et al. Quantification of target gene expression by imaging reporter gene expression in living animals. Nat Med 2000;6:933–7.
19. Jacobs A, Dubrovin M, Hewett J, et al. Functional coexpression of HSV-1 thymidine kinase and green fluorescent protein: implications for noninvasive imaging of transgene expression. Neoplasia 1999;1:154–61.
20. Aghi M, Kramm CM, Chou TC, Breakefield XO, Chiocca EA. Synergistic anticancer effects of ganciclovir/thymidine kinase and 5-fluorocytosine/cytosine deaminase gene therapies. J Natl Cancer Inst 1998;90:370–80.
21. Machulla HJ, Blocher A, Kuntzsch M, Piert M, Wei R, Grierson JR. Simplified labeling approach for synthesizing 3′-deoxy-3′-[^{18}F]fluorothymidine ([^{18}F]FLT). J Radioanal Nucl Chem 2000;243:843–6.
22. Wodarski C, Eisenbarth J, Weber K, Henze M, Haberkorn U, Eisenhut M. Synthesis of 3-deoxy-3-[^{18}F]fluoro-thymidine with 2,3-anhydro-5-*O*-(4,4-dimethoxytrityl)-thymidine. J Labelled Cpd Radiopharm 2000;43:1211–8.
23. Heiss WD, Pawlik G, Herholz K, Wagner R, Goldner H, Wienhard K. Regional kinetic constants and cerebral metabolic rate for glucose in normal human volunteers determined by dynamic positron emission tomography of [^{18}F]-2-fluoro-2-deoxy-D-glucose. J Cereb Blood Flow Metab 1984;4:212–23.
24. Herholz K, Holzer T, Bauer B, et al. ^{11}C-methionine PET for differential diagnosis of low-grade gliomas. Neurology 1998;50:1316–22.
25. Cizek J, Herholz K, Vollmar S, Schrader R, Klein J, Heiss WD. Fast and robust registration of PET and MR images of human brain. Neuroimage 2004;22:434–42.
26. Alauddin MM, Conti PS. Synthesis and preliminary evaluation of 9-(4-[^{18}F]-fluoro-3-hydroxymethylbutyl)-guanine ([^{18}F]FHBG): a new potential imaging agent for viral infection and gene therapy using PET. Nucl Med Biol 1998;25:175–80.
27. Yaghoubi S, Barrio JR, Dahlbom M, et al. Human pharmacokinetic and dosimetry studies of [(18)F]FHBG: a reporter probe for imaging herpes simplex virus type-1 thymidine kinase reporter gene expression. J Nucl Med 2001;42:1225–34.
28. Jacobs A, Tjuvajev JG, Dubrovin M, et al. Positron-emission tomography-based imaging of transgene expression mediated by replication-conditional, oncolytic herpes simplex virus type 1 mutant vectors *in vivo*. Cancer Res 2001;61:2983–95.
29. Sandmair AM, Loimas S, Puranen P, et al. Thymidine kinase gene therapy for human malignant glioma, using replication-deficient retroviruses or adenoviruses. Hum Gene Ther 2000;11:2197–205.
30. Trask TW, Trask RP, Aguilar-Cordova E, et al. Phase I study of adenoviral delivery of the HSV-tk gene and ganciclovir administration in patients with current malignant brain tumors. Mol Ther 2000;1:195–203.
31. Jacobs AH, Voges J, Kracht LW, et al. Imaging in gene therapy of patients with glioma. J Neurooncol 2003;65:291–305.
32. Harsh GR, Deisboeck TS, Louis DN, et al. Thymidine kinase activation of ganciclovir in recurrent malignant gliomas: a gene-marking and neuropathological study. J Neurosurg 2000;92:804–11.
33. Haberkorn U, Bellemann ME, Gerlach L, et al. Uncoupling of 2-fluoro-2-deoxyglucose transport and phosphorylation in rat hepatoma during gene therapy with HSV thymidine kinase. Gene Ther 1998;5:880–7.
34. Pantuck AJ, Berger F, Zisman A, et al. CL1-39: a noninvasive molecular imaging model of prostate cancer suicide gene therapy using positron emission tomography. J Urol 2002;168:1193–8.
35. Soling A, Theiss C, Jungmichel S, Rainov NG. A dual function fusion protein of herpes simplex virus type 1 thymidine kinase and firefly luciferase for noninvasive *in vivo* imaging of gene therapy in malignant glioma. Genet Vaccines Ther 2004;2:7.
36. Yaghoubi SS, Barrio JR, Namavari M, et al. Imaging progress of herpes simplex virus type 1 thymidine kinase suicide gene therapy in living subjects with positron emission tomography. Cancer Gene Ther 2005;12:329–39.
37. Barton KN, Tyson D, Stricker H, et al. GENIS: gene expression of sodium iodide symporter for noninvasive imaging of gene therapy vectors and quantification of gene expression *in vivo*. Mol Ther 2003;8:508–18.
38. Qiao J, Doubrovin M, Sauter BV, et al. Tumor-specific transcriptional targeting of suicide gene therapy. Gene Ther 2002;9:168–75.
39. De A, Lewis XZ, Gambhir SS, Noninvasive imaging of lentiviral-mediated reporter gene expression in living mice. Mol Ther 2003;7:681–91.
40. Davidson BL, Breakefield XO. Viral vectors for gene delivery to the nervous system. Nat Rev Neurosci 2003;4:353–64.
41. Cunningham C, Davison AJ. A cosmid-based system for constructing mutants of herpes simplex virus type 1. Virology 1993;197:116–24.
42. Saeki Y, Breakefield XO, Chiocca A. Improved HSV-1 amplicon packaging system using ICP27-deleted, oversized HSV-1 BAC DNA. Methods Mol Med 2003;76:51–60.
43. Costantini LC, Fraefel C, Breakefield XO, Isacson O. Herpes simplex virus/adeno-associated virus hybrid vectors for gene transfer to neurons. Preparation and use. Methods Mol Med 2002;69:479.
44. Johnston KM, Jacoby DR, Pechan PA, et al. HSV/AAV hybrid amplicon vectors extend transgene expression in human glioma cells. Hum Gene Ther 1997;8:359–70.
45. Alauddin MM, Shahinian A, Gordon EM, Bading JR, Conti PS. Preclinical evaluation of the penciclovir analog 9-(4-[^{18}F]Fluoro-3-hydroxymethylbutyl)guanine for *in vivo* measurement of suicide gene expression with PET. J Nucl Med 2001;42:1682–90.
46. Black ME, Newcomb TG, Wilson HM, Loeb LA. Creation of drug-specific herpes simplex virus type 1 thymidine kinase mutants for gene therapy. Proc Natl Acad Sci U S A 1996;93:3525–9.
47. Moolten FL, Tumor chemosensitivity conferred by inserted herpes thymidine kinase genes: paradigm for a prospective cancer control strategy. Cancer Res 1986;46:5276–81.
48. Freeman SM, Abboud CN, Whartenby KA, et al. The "bystander effect": tumor regression when a fraction of the tumor mass is genetically modified. Cancer Res 1993;53:5274–83.
49. Mullen CA, Kilstrup M, Blaese RM. Transfer of the bacterial gene for cytosine deaminase to mammalian cells confers lethal sensitivity to 5-fluorocytosine: a negative selection system. Proc Natl Acad Sci U S A 1992;89:33–7.
50. Fischer U, Steffens S, Frank S, Rainov NG, Schulze-Osthoff K, Kramm CM. Mechanisms of thymidine kinase/ganciclovir and cytosine deaminase/ 5-fluorocytosine suicide gene therapy-induced cell death in glioma cells. Oncogene 2005;24:1231–43.
51. Freytag SO, Rogulski KR, Paielli DL, Gilbert JD, Kim JH. A novel three-pronged approach to kill cancer cells selectively: concomitant viral, double suicide gene, and radiotherapy. Hum Gene Ther 1998;9:1323–33.
52. Rogulski KR, Kim JH, Kim SH, Freytag SO. Glioma cells transduced with an *Escherichia coli* CD/HSV-1 TK fusion gene exhibit enhanced metabolic suicide and radiosensitivity. Hum Gene Ther 1997;8:73–85.
53. Moriuchi S, Wolfe D, Tamura M, et al. Double suicide gene therapy using a replication defective herpes simplex virus vector reveals reciprocal interference in a malignant glioma model. Gene Ther 2002;9:584–91.
54. Grierson JR, Shields AF. Radiosynthesis of 3′-deoxy-3′-[(18)F]fluorothymidine: [(18)F]FLT for imaging of cellular proliferation *in vivo*. Nucl Med Biol 2000;27:143–56.
55. Mier W, Haberkorn U, Eisenhut M. [^{18}F]FLT; portrait of a proliferation marker. Eur J Nucl Med Mol Imaging 2002;29:165–9.
56. Shields AF, Grierson JR, Dohmen BM, et al. Imaging proliferation *in vivo* with [F-18]FLT and positron emission tomography. Nat Med 1998;4:1334–6.
57. Schwartz JL, Tamura Y, Jordan R, Grierson JR, Krohn KA. Monitoring tumor cell proliferation by targeting DNA synthetic processes with thymidine and thymidine analogs. J Nucl Med 2003;44:2027–32.
58. Wagner M, Seitz U, Buck A, et al. 3′-[^{18}F]fluoro-3′-deoxythymidine ([^{18}F]-FLT) as positron emission tomography tracer for imaging proliferation in a murine B-Cell lymphoma model and in the human disease. Cancer Res 2003;63:2681–7.
59. Choi SJ, Kim JS, Kim JH, et al. [([18])F]3′-deoxy-3′-fluorothymidine PET for the diagnosis and grading of brain tumors. Eur J Nucl Med Mol Imaging 2005;32:653–9.
60. Jacobs AH, Thomas A, Kracht LW, et al. ^{18}F-Fluoro-L-thymidine and ^{11}C-methylmethionine as markers of increased transport and proliferation in brain tumors. J Nucl Med 2005;46:1948–58.
61. Chen W, Cloughesy T, Kamdar N, et al. Imaging proliferation in brain tumors with ^{18}F-FLT PET: comparison with ^{18}F-FDG. J Nucl Med 2005;46:945–52.
62. Dittmann H, Dohmen BM, Kehlbach R, et al. Early changes in [^{18}F]FLT uptake after chemotherapy: an experimental study. Eur J Nucl Med Mol Imaging 2002;29:1462–9.
63. Johnson M, Sato M, Burton J, Gambhir SS, Carey M, Wu L. Micro-PET/CT monitoring of herpes thymidine kinase suicide gene therapy in a prostate cancer xenograft: the advantage of a cell-specific transcriptional targeting approach. Mol. Imaging 2005;4:463–72.
64. Hajitou A, Trepel M, Lilley CE, et al. A hybrid vector for ligand-directed tumor targeting and molecular imaging. Cell 2006;125:385–98.

Downloaded from http://aacrjournals.org/cancerres/article-pdf/67/4/1706/2578556/1706.pdf by guest on 09 December 2023